



1 **Enhancing drought monitoring and assessment capability in** 2 **India through high-resolution (250m) data**

3 Anukesh Krishnankutty Ambika¹ and Vimal Mishra^{1,2}

4
5 ¹Earth Sciences, Indian Institute of Technology (IIT) Gandhinagar
6 ²Civil Engineering, Indian Institute of Technology (IIT) Gandhinagar

7
8 *Correspondence to:* vmishra@iitgn.ac.in

9 **Abstract**

10

11 Drought poses a tremendous challenge to India's socioeconomic development, livelihood,
12 agriculture, and water management. While existing drought monitoring systems have
13 characterized drought impact at different scales, policymaking and management require
14 drought assessment at sub-district or taluka (sub-district) levels. Here, we develop high-
15 resolution (250 m) agriculture drought indices for the Indian region to overcome the
16 shortcomings of the coarse resolution datasets. We used the co-kriging to downscale the Land
17 Surface Temperature (LST) from 1000m to 250m. The LST and Enhanced Vegetation Index
18 (EVI) are obtained at 8-day intervals at 250m spatial resolution. The high-resolution datasets
19 show significant improvement in identifying the severity and coverage of drought. Soil
20 Moisture Agriculture Drought Index (SMADI), which accounts for water stress and
21 vegetation lag response, shows high reliability in drought detection. We evaluated drought
22 extent and severity using the newly developed dataset and found that the high-resolution
23 dataset can be used to separate the irrigation impact on drought alleviation. The high-
24 resolution drought indices from SMADI and the Normalized Vegetation Supply Water Index
25 (NVSWI) effectively represent the drought conditions at district and taluka levels that can be
26 used in drought impacts assessments in India.

27 **1 Introduction**

28

29 Drought is one of the complex natural hazards (Lloyd-Hughes, 2014; Van Loon, 2015;
30 Wilhite et al., 2000), which poses tremendous challenges to water resources management,
31 agriculture, and Gross Domestic Product (GDP) due to a sustained deficit of water
32 availability (Godfray et al., 2010; Mooley and Parthasarathy, 1983; Wilhite, 2005). The
33 vulnerability of the Indian population to drought is relatively high due to economic viability
34 from the agriculture sector (Mishra and Singh, 2010). The recent increase in temperature and



35 erratic summer monsoon have impacted the frequency, intensity, and areal extent of drought
36 over the Indian region (Mishra et al., 2012; Roxy et al., 2015). Moreover, the frequency of
37 flash drought has also increased in recent decades (Mahto and Mishra, 2020). For example,
38 ten major droughts occurred between 1950 and 1989, while five occurred after 2000 (Mishra,
39 2020). The frequency of flash drought is projected to increase seven-fold by the end of the
40 21st century, with a considerable economic implications (Mishra et al., 2021). For instance,
41 the 2014-2015 drought resulted in the loss of billions of dollars affecting more than 3.3
42 million people in India (Mishra et al., 2018). Therefore, quantifying drought impacts at high
43 resolution is necessary for water management and food security.

44

45 Meteorological, agricultural, hydrological, and socioeconomic droughts (Wilhite and Glantz,
46 1985) are propagated and intensified through land-atmospheric interactions, local land
47 surface characteristics, soil moisture availability, regional climate change, and human
48 interferences (Barker et al., 2016; Van Loon and Laaha, 2015; Mishra et al., 2021; Shah et
49 al., 2021). The temporal characteristics, area affected, extent, frequency, severity, intensity,
50 and duration of drought are characterized by several drought indices (Dai, 2011; Mishra et
51 al., 2016; Yu et al., 2014). Drought characteristics are monitored using Standardized
52 Precipitation index [SPI; (McKee et al., 1993)] and Standardized Precipitation
53 Evapotranspiration Index [SPEI; (Vicente-Serrano et al., 2010)], which incorporate the
54 influence of precipitation, temperature, and evapotranspiration on drought estimates.
55 Moreover, the Palmer drought Severity Index (PDSI) takes into account soil water balance to
56 identify drought by considering the potential loss of moisture due to temperature (Palmer,
57 1965). Further, Standardized Soil Moisture Index [SSMI; (Hao and AghaKouchak, 2013)]
58 and Standardized Streamflow Index [SSI; (Bhardwaj et al., 2020)] are widely used for
59 agricultural and hydrological droughts, respectively. Although these indices may provide
60 valuable information on drought, high uncertainties exist in drought detection due to sparse
61 weather stations and spatial interpolation.

62

63 Several drought monitoring, warning, and prediction related measures are relatively less
64 developed than the other major disasters due to the complexity of the process involved in
65 identifying and propagating drought (Saha et al., 2021). Drought impact assessment-related
66 efforts in India are limited due to a lack of fine-scale/higher resolution information that can
67 resolve sub-district level characteristics (Shah and Mishra, 2015). For instance, the near real-



68 time drought monitoring in South Asia at 0.05° indicated that the bias-corrected high-
69 resolution datasets effectively capture observed drought variability, similar to information
70 obtained by satellite remote sensing (Aadhar and Mishra, 2017). The near real-time drought
71 system for the Indian region considers meteorological information (Shah and Mishra, 2015).
72 India Meteorological Department (IMD) provides monthly scale drought information at
73 relatively coarser resolution (www.imdpune.gov.in), which is helpful for the decision making
74 at the administrative level (district). Furthermore, satellite-based near real-time drought
75 monitoring and early warning systems provide a drought warning at the state level (Takeuchi
76 et al., 2015). Bias corrected high-resolution near real-time drought monitoring at 0.05°
77 provides the severity of drought over South Asia (Aadhar and Mishra, 2017). While the
78 existing drought monitoring system in the Indian region offers important information on
79 drought, decision-making at the local level is hindered due to their coarse spatial resolution.
80 Therefore, remote sensing-based high-resolution drought monitoring can be used as a
81 supplement to garner the spatial variability of drought impact.

82 Vegetation indices are commonly used satellite-based drought monitoring at high resolution
83 (Bannari et al., 1995). Moreover, vegetation stress indices incorporating ecosystem
84 components are more prominent for drought detection (Jiao et al., 2021). Although the
85 vegetation stress alone can indicate drought onset and termination (Agutu et al., 2017),
86 combining land surface temperature improves the drought prediction due to the changes in
87 local biophysical (soil, slope) and climate conditions (García-León et al., 2019). Moreover,
88 the additive impact of surface temperature and vegetation stress is highly correlated with the
89 crop yield in various agro-meteorological zones (Kogan et al., 2012; Prasad et al., 2006;
90 Rahman et al., 2009). Since agricultural drought is modulated by the land surface condition,
91 separating irrigation impact on the cropping area is crucial for identifying the drought extent
92 (Mishra et al., 2016) as irrigation modulates the vegetation health and surface temperature
93 during the summer (Ambika and Mishra, 2019). In addition, various vegetation-related
94 remote sensing drought indices that combine surface temperature with vegetation conditions
95 can be a viable indicator in monitoring agricultural drought (Bento et al., 2018; Gomes et al.,
96 2017; Rojas et al., 2011). High-resolution drought monitoring at a regional scale can also be
97 valuable for decision making at sub-district (Taluka) levels.

98 Land surface temperature (LST) is one of the critical parameters for an integrated high-
99 resolution drought monitoring system since it indirectly measures surface energy balance



100 (Tomlinson et al., 2011). Thermal stress is a good indicator for early drought detection,
101 derived from LST (Anderson et al., 2008; Seyednasrollah et al., 2019). The combination of
102 LST and EVI indices can be an excellent indicator for multi-sensor drought detection and
103 monitoring strategies (Orhan et al., 2014). The relation between thermal stress and vegetation
104 condition has been successfully applied for drought monitoring (Seyednasrollah et al., 2019).
105 Further, while combining with other metrics like soil moisture, the LST-EVI relationship has
106 shown potential for improved drought monitoring (Hao et al., 2015; Jiao et al., 2019).

107 We develop a high-resolution drought index using LST and EVI at 250 m resolution. We
108 developed Vegetation Health Index (VHI), Vegetation Condition Index (VCI), Temperature
109 Condition Index (TCI), Normalized vegetation Supply Water Index (NVSWI), and Soil
110 Moisture Agriculture Drought Index (SMADI) at 250 m. Moderate Resolution Imaging
111 Spectroradiometer (MODIS) datasets were used to develop eight-day continuous LST and
112 enhanced vegetation index (EVI). The high-resolution agriculture drought dataset at 250 m
113 resolution at the national scale can be used for impact assessment.

114 **2 Methods**

115 **2.1 Enhanced Vegetation Index (EVI) at 8-day interval**

116 The Enhanced Vegetation Index (EVI) can identify the variation in leaf area index (LAI),
117 canopy cover, and photosynthetically active radiation (Gao et al., 2000). Therefore, EVI is
118 useful in monitoring seasonal, inter-annual, and inter-annual long-term variation in vegetation
119 stress (Huete et al., 2002). Moreover, the blue wavelength corrections for distortion make
120 EVI not saturate quickly, as is the case of the Normalized Difference Vegetation Index
121 (NDVI) [Gao et al., 2000]. Further, EVI is sensitive to the green biomass response in varying
122 weather conditions. EVI from MODIS provides global coverage at a sixteen-day interval with
123 a better spectral, spatial, geometric, and radiometric quality (Didan et al., 2015). Moreover, 8-
124 day EVI can detect vegetation response to changes in atmospheric vapour pressure deficit,
125 clouds, and sun view angles (Gurung et al., 2009). We developed the 8-day MODIS EVI
126 temporal composite at 250 m for the 2000–2017 period. We used daily MOD09Q1 [Red (620-
127 720 nm) and Near Infrared (841–876 nm)] at 250 m and MOD09A1 (Blue 459–479 nm) at
128 500 m surface reflectance. The MOD09A1 Band-3 is resampled using the nearest neighbour
129 to keep the spatial consistency of the raw dataset. The eight-day composite is derived from
130 the datasets corrected for atmospheric conditions like aerosol, Rayleigh scattering, and
131 gasses. EVI at 250 resolution is obtained using the same algorithm provided for the EVI



132 (Didan et al., 2015). The abbreviation and the summary of datasets used in the study are
133 given in Tables 1 and 2.

134

135 **2.2 Downscaling Land Surface Temperature (LST) data at 250 m**

136 There have been numerous satellite LST observations in recent decades with limited spatial
137 and temporal resolution (Gutman, 1999; Li et al., 2014), restricting their use to broader
138 hydrological applications. For example, the National Oceanic and Atmospheric
139 Administration (NOAA) Star Center for Satellite Application and Research (NSTAR)
140 provide weekly LST at 4 km spatial resolution from 1982 to 2018 (Tomlinson et al., 2011).
141 However, ASTER satellite data at 90 m spatial resolution revisit the same area every 16 days.
142 Therefore, a high-resolution (spatial and temporal) LST dataset adds value to drought
143 monitoring.

144 We downscaled MODIS (MOD11A2) LST 1000 m to 250 m using the co-kriging method
145 (Pardo-Igúzquiza et al., 2006). The downscaled LST was then combined with EVI to evaluate
146 various drought indices over India. The 8-day MODIS data product MOD11A2 land surface
147 temperature (LST) corresponds to an average value for the period. The improvement in
148 version 6 of the MODIS LST uses a split-window algorithm with comprehensive regression
149 analysis, reducing LST uncertainties' sensitivity (Wan, 2006). All the MODIS granules over
150 the Indian region were mosaicked and reprojected to the geographic coordinates system using
151 the NASA reprojection tool (mrtweb.cr.usgs.gov).

152 Downscaling combines two or more data sets of different spatial resolutions to derive an
153 enhanced resolution dataset (Pardo-Iguzquiza et al., 2011). Previous studies have used
154 empirical relations between visible, near-infrared, and shortwave infrared (SWIR) bands and
155 Vegetation Index (NDVI or EVI) for high resolution (Agam et al., 2007; Gowda et al., 2007;
156 Jeganathan et al., 2011; Nichol and Wong, 2005). However, downscaling provides promising
157 results since it preserves the variation of ground features and maintains image geometry
158 coherence (Rodriguez-Galiano et al., 2012). The correlation between LST and spectral bands
159 is low (Rodriguez-Galiano et al., 2012). However, a joint variability pattern can be observed
160 between the LST and the spectral bands (Drury, 1987). Further, LST can be downscaled
161 using the joint variability of the cross-covariance (Liu et al., 2006). We used co-kriging as an
162 approximation method with the high-resolution data to downscale the LST (Stathopoulou and
163 Cartalis, 2009). Previous studies using experimental cross-covariances and direct covariances



164 showed promising results in downscaling Landsat LST (Agam et al., 2007). The Cokriging
165 considers the pixel size and the sensor's point-spread function to calculate the weights for
166 downscaling, which is an added advantage compared to other methods (Kustas et al., 2003).
167 Hence, the downscaled image preserves the spatial and radiometric variability (Rodriguez-
168 Galiano et al., 2012). Further, the cokriging ensures identical spatial variability of the raw
169 datasets even when the point-scale function degrades the spatial coherence (Liu et al., 2006;
170 Rodriguez-Galiano et al., 2012; Stathopoulou and Cartalis, 2009).

171 Downscaling of LST is processed with EVI and Shuttle Radar Topography Mission (SRTM)
172 elevation datasets as covariates. The SRTM elevation is resampled with cubic convolution at
173 250 m to maintain spatial consistency. Since the elevation is one of the prominent factors in
174 changing the land surface temperature, we used SRTM elevation as another covariate.
175 Further, the Indian subcontinent is divided into 1200 tiles, with each tile covering an area
176 coverage of approximately 0.34 million hectares (mha). The majority of tiles are confined to
177 an individual agro-ecological zone. The downscaling weights were calculated from both
178 covariates to downscale LST at 250 m.

179 The downscaled LST was evaluated against 1km LST using structural similarity index
180 [SSIM; (Wang et al., 2004)]. SSIM evaluates image quality based on luminescence, contrast,
181 and structural differences between the degraded (high resolution) image and the original
182 image (low resolution). SSIM ranges between -1 and 1, with values closer to 1 showing better
183 similarity (Rodriguez-Galiano et al., 2012). The image quality index (IQI) was also used
184 (Wang and Bovik, 2002) to account for luminance distortion, loss of correlation, and contrast
185 distortion [Table S2]. The quality of the downscaled data was evaluated for different regions
186 in India using districts and talukas boundaries.

187

188 **2.3 High-Resolution vegetation Indices**

189 We calculated various agriculture drought indices from the downscaled LST and EVI at 250
190 m. First, we obtained the Vegetation Condition Index (VCI), which indicates the vegetation
191 stress and is the most commonly used agriculture drought index (Kogan, 1995a). VCI can
192 isolate the weather-related vegetation stress and detect the drought onset, intensity, and
193 impact on vegetation (Kogan, 1995a). Unlike VCI, Temperature Condition Index (TCI)
194 determines the vegetation stress caused by temperature and excessive wetness. We calculated



195 both indices for the 2000-2017 period (Kogan, 1995a). Even though the VCI and TCI are
196 effective indicators for drought detection, combining both indices could be more effective in
197 determining the drought intensity (Kogan, 1995a; Rojas et al., 2011). For example, the
198 Vegetation Health Index (VHI) is an additive combination of VCI and TCI for drought
199 detection. Moreover, Kogan (1995) proposed VHI to remove cloud effects from the
200 Advanced Very High-Resolution Radiometer (AVHRR) thermal band (Kogan, 1995a,
201 1995b). Therefore, VHI indicates drought for seasons having high temperatures and
202 favourable conditions for low temperatures.

203 Soil moisture plays a crucial role in drought detection and identification (Seneviratne et al.,
204 2010). Integrating soil moisture in drought indices enhances our understanding of land-
205 atmospheric interaction in modulating the drought event (Seneviratne et al., 2010). We
206 calculated the Soil Moisture Agricultural Drought Index (SMADI) by combining surface
207 temperature conditions, lagged response of vegetation, and soil moisture to detect the short-
208 term drought (Sánchez et al., 2016). The SMADI can provide early warning of yield
209 reduction due to its sensitivity to water stress (Souza et al., 2021). Surface soil moisture for
210 the SMADI index is obtained from the Global Land Evaporation Amsterdam Model
211 (GLEAM; 0.25°) at a 10 cm depth and resampled at a resolution of 250 m. We used the
212 nearest neighbour resampling method to keep the spatial consistency with the original
213 dataset. The GLEAM v3.2a soil moisture uses extensive validation against the in-situ data
214 points having higher accuracy than other data GLEAM v3.2b (Martens et al., 2017). To
215 compensate for the SMADI response towards drought, we calculated the Normalized
216 vegetation Supply Water Index [NVWSI; (Abbas et al., 2014)]. The NVSWI assumes that
217 land surface temperature will be low when sufficient soil water supply exists (Abbas et al.,
218 2014). However, during the dry condition, the leaf stomata are partly closed to sustain water
219 stress, resulting in a reduction in evapotranspiration and increased surface temperature (Zhou
220 et al., 2019). Hence, the NVSWI depends on vegetation health and indirectly indicates the
221 soil moisture-induced drought changes.

222

223 We used the Standardized Evaporation Deficit Index [SEDI - 0.25°; (Vicente-Serrano et al.,
224 2018)] and Drought Severity Index [DSI - 0.05° & 0.25°; (Mu et al., 2013)] to evaluate the
225 drought estimates from NVSWI and VHI for the Indian Region. The derived drought indices
226 were aggregated to 0.05° using the majority resampling techniques to compare drought
227 extent. We used ranges of indicators to categorize drought as incipient drought (between -0.5



228 and -0.59), mild drought (between -0.6 and -0.89), moderate drought (between -0.9 and -
229 1.19), severe drought (between -1.2 and -1.49), and extreme drought (between -1.5 and less).

230

231 **3 Result and Discussion**

232

233 **3.1 Land Surface temperature at 250 m resolution**

234

235 First, we evaluated the quality of the downscaled LST at 250m during February 2000 (Fig. 1).

236 We observed that the high-resolution and coarse-resolution LST display similar SSIM and

237 IQM over the selected region of central India (Fig. 1b,c). However, as expected, LST at 250

238 m displays greater spatial details, useful for drought assessment (Fig. S2 & S3). The

239 downscaled LST indicates geographic variability, considering using the SRTM elevation data
240 (Fig. S3). To evaluate the spatial variability of drought, areas from diverse climatic settings

241 were selected. Initially, the LST was downscaled using EVI as a covariate, indicating lesser

242 SSIM (Fig. S2). Furthermore, downscaling LST by EVI and elevation dataset as a covariate

243 improved the spatial dispersion coherently (Fig S2). The structural variability of LST

244 enhanced significantly from single to multi covariate downscaling (Fig. S2). Moreover, by

245 including multiple covariates, the co-kriging improved the coherence of the spatial continuity

246 in downscaled LST (Rodriguez-Galiano et al., 2012). Further, we considered an area

247 characterized by various natural land covers, with vegetation mixtures, build-up, cropping

248 area, bare soils, and urban land area to evaluate the spatial variance in LST downscaling. All

249 the downscaled images were identical to the original 1000m, indicating less bias in tone,

250 contrast, and saturation [Fig. S4 & S5; Table. S1 & S2]. However, the downscaled image

251 showed a consistent mean value of LST with variation in standard deviation. Our results

252 show a good agreement between 250 m and 1000 m LST with a mean SSIM value of 0.52 for

253 district and taluka boundary areas (Table S1). Further, the IQI shows less luminance and

254 contrast distortion with a high correlation. Both district and taluka levels have a higher degree

255 of confidence between 250 m and 1000 m LST with a mean value of 0.86 (Table S2). The

256 downscaled LST signifies variation in continuity as it is expected that high-resolution

257 datasets represent higher spatial variability than low-resolution with lesser pixel numbers

258 (Pardo-Iguzquiza et al., 2011; Pardo-Igúzquiza et al., 2006). In general, the downscaled LST

259 can be used with EVI of the same resolution for monitoring the agriculture drought at 250

260 m.

261

262 **3.2 Drought assessment at different resolutions**



263 Next, we estimated the area under drought for DSI and SEDI from 2000 to 2011. We
264 observed that drought impacts around 10% of the Indian region each year. Moderate-
265 resolution (0.05°) DSI and low-resolution SEDI (0.25°) were analyzed to understand the
266 variability in drought severity (Fig. 2a,b). As expected, DSI at 0.05° shows a reasonable
267 improvement in capturing the spatial and temporal variability of drought-affected areas
268 during 2000–2011. DSI integrates remotely sensed NDVI, potential evapotranspiration, and
269 evapotranspiration (Mu et al., 2013). Moreover, DSI incorporates vegetation response to the
270 dry condition and terrestrial water availability associated with dryness or wetness (Mu et al.,
271 2013). Further, we selected different drought-affected areas to evaluate the spatial extent of
272 drought severity change at different resolutions. The eight-day dataset of DSI identified the
273 mesoscale geographical variability of the severe drought period compared to the SEDI, which
274 is available at a monthly scale (Fig. 2 c-f & g-j). We note DSI and SEDI follow a similar
275 pattern of the area under drought (Fig. 2a, b). Since SEDI exhibits a higher correlation with
276 the vegetation anomalies, SEDI identifies water stress sensitivity to leaf activity (Vicente-
277 Serrano et al., 2018). Moreover, SEDI is formulated based on the evaporative deficit, which
278 signifies a similar spatial extent of drought as DSI. The spatial severity of drought in DSI
279 indicates that high-resolution datasets can improve the understanding of drought impacts. For
280 example, the NDVI and LST at 250m can separate the drought impact in irrigated and rainfed
281 areas (Ambika and Mishra, 2019). The drought severity analysis by combining model output
282 with observation highlights the uncertainty in percentage area under drought (Aadhar and
283 Mishra, 2017). Hence, the noticeable difference in extreme drought-impacted areas in DSI
284 and SEDI emphasizes accounting for the spatial variability of drought.

285 We selected four areas highlighted during the significant drought period to quantify the
286 spatial variability of drought extent at high-resolution (Fig. 2 c-f). We compared 0.25° and
287 0.05° DSI with 250 m NVSWI and VHI (Fig. 3). The difference in the spatial variability of
288 drought shows the bias in drought extent at a coarser resolution (Fig. 3q). For instance, the
289 NVSWI and VHI show relatively low values for the drought extent during 2002 and 2005
290 compared to 2000 and 2009. Further, during 2009 the DSI underestimated drought extent by
291 45%. Based on the 12-month SPI and SPEI at 0.05° , drought analysis identifies 40-50% of
292 Bulandshahr district under severe drought during 2015 (Aadhar and Mishra, 2017). On the
293 other hand, the same analysis at 0.05° eliminates the drought condition in other districts
294 [Faisalabad and Ratnapura; (Aadhar and Mishra, 2017)], which further indicates the utility of
295 high-resolution drought monitoring to identify the macroscale variability.



296

297 **3.3 Temporal variability in agriculture drought**

298 Most of the Indian region underwent different drought events during the past decades. One of
299 the deadliest meteorological droughts lasted from 2000 to 2003 (Mishra, 2020). During 2002
300 the drought was caused by a precipitation deficit of 21.5% during the summer monsoon
301 season. Further, in July, a precipitation deficit of 56% had a devastating impact on the
302 socioeconomic environment (Mishra, 2020). Considering these, we used the 2002 summer as
303 a case study to evaluate the spatial pattern detected in the newly developed high-resolution
304 drought indices.

305 We identified drought during 2002 March and compared the spatial extent of all the indices.
306 DSI and SEDI show a similar drought extent and are more prominent over the Indo-Gangetic
307 plain and Deccan plateau (Fig. S6). Further, irrigation-induced alleviation of agriculture
308 stress is not observed in the DSI and SEDI. For instance, Ambika et al. (2019) identified that
309 the vegetation stress on peak growing period is significantly reduced by irrigation. NVSWI
310 and VHI show similar vegetation stress changes along the Indo-Gangetic plain (Fig S6). the
311 Multi-index drought at 250m shows consistency in drought severity extent (Fig. 4). However,
312 the soil moisture-induced SMADI shows a more prominent impact of drought (Fig. 4e-h).
313 The existence of soil moisture and lagged response of agriculture stress in SMADI can
314 characterize the drought condition, particularly in areas where crop yield is more sensitive to
315 water stress (Souza et al., 2021). We identified a similar extent of drought severity in NVSWI
316 and SMADI along the Indian region, indicating that soil moisture has lagged response to
317 vegetation stress [Fig. 5; (Gurung et al., 2009)]. Moreover, all the drought indices at 250 m
318 show a similar pattern of spatial extent during September 2002. The comparisons of multi-
319 index drought at 250m show that the areal extent and severity of drought at high-resolution
320 are necessary for management at the taluka (sub-district) level.

321 Finally, we developed district and taluka level maps of drought severity and the extent to
322 understand the applicability in assisting decision-making (Fig. 6). We considered the 2015
323 drought to evaluate the vegetation drought response. The meteorological drought in 2015 was
324 the longest in the entire record of a century and peaked in June 2016 (Mishra, 2020). The
325 2016 drought affected more than 16% of the country but was less severe than the other
326 meteorological drought (Mishra, 2020). The 8-day high-resolution drought obtained from the
327 NVSWI and SMADI shows that a large area of central India experienced severe and extreme



328 drought (Fig. 6a, b). Further, the highlighted maps of district and taluka level under drought
329 severity show the consistent extent in SMADI and NVSWI, which can be used for decision
330 and policymaking (Fig. 6c-f).

331

332 **4 Data availability**

333 The high-resolution LST and NVSWI are publicly available from the Zenodo versions link:
334 <https://doi.org/10.5281/zenodo.6798442>. The dataset covers the Indian region at 8-day
335 temporal resolution at 250 m spatial resolution for the 2000 – 2017 period. The dataset is
336 provided in WGS 1984 projection and tiff format.

337

338 **5 Conclusions**

339 The current study presents a newly developed high-resolution land surface temperature and
340 enhanced vegetation index dataset at an 8-day interval with 250 m resolution over the Indian
341 region. Further, we developed different agriculture drought indices (VCI, TCI, VHI, NVSWI,
342 and SMADI) at 250 m. The data is derived from satellite-based MODIS and GLEAM surface
343 soil moisture covering the entire Indian region from 2000 to 2017. The eight-day dataset is
344 provided to facilitate characterization of drought severity and extent at high resolution.
345 Moreover, the increased frequency of drought monitoring helps to characterize agricultural
346 drought at high temporal resolution for the Indian region. The high-resolution drought indices
347 show significant improvement in detecting drought extent and severity. The multi-index
348 drought can characterize the drought impact at district and taluka (sub-district) boundaries.

349 The inclusion of soil moisture in SMADI accounts for the water stress, and lag response
350 highlights drought severity. SMADI and NVSWI show high reliability in investigating
351 drought detection capability at the district and taluka levels. The high-resolution multi-index
352 drought can act as an early warning to drought detection and mitigation compared to the other
353 hydrological, meteorological and socioeconomic drought indices. The high-resolution dataset
354 exhibits the potential to separate the land management impact on the drought alleviation—for
355 instance, the extensive irrigation in the Indo-Gangetic plain. These results highlight the
356 validity and advantage of high-resolution drought monitoring, and its unprecedentedly high
357 resolution offers critical benefits to monitoring and assessment for policy and decision-
358 makers.



359

360 **Acknowledgement:** Authors appreciate the Ministry of Human Resources Development
361 (MHRD). The authors acknowledge the data availability from the Moderate Resolution
362 Imaging Spectroradiometer (MODIS). Land Surface Temperature (LST), Enhanced
363 Vegetation Index (EVI) and all the ancillary can be obtained from
364 <https://e4ftl01.cr.usgs.gov/>. The Global Land Evaporation Amsterdam Model (GLEAM) soil
365 moisture can be obtained from <https://www.gleam.eu/#downloads>. The global gridded
366 monthly Standardized Evaporation Deficit Index (SEDI) and Drought Severity Index (DSI)
367 can be downloaded from <https://digital.csic.es/handle/10261/160091> and
368 http://files.nts.g.umt.edu/data/NTSG_Products/DSI/ (<https://larsjung.de/h5ai/>) (umt.edu). The
369 global map of irrigated area version 5 was collected from
370 [https://www.fao.org/aquastat/en/geospatial-information/global-maps-irrigated-areas/latest-](https://www.fao.org/aquastat/en/geospatial-information/global-maps-irrigated-areas/latest-version/)
371 [version/](https://www.fao.org/aquastat/en/geospatial-information/global-maps-irrigated-areas/latest-version/). The global irrigated temporal map of fractional Historic Irrigation Datasets can be
372 obtained from <https://mygeohub.org/publications/8/2>.

373 **Code Availability:** Codes used to develop the high-resolution datasets can be obtained from
374 the corresponding author.

375 **Competing interests:** Authors declare no competing interest.

376 **Author contributions:** VM and AKM designed the study. AKA developed the dataset and
377 wrote the initial draft. VM and AKA discussed results and enhanced the initial draft.

378 References

379

380 Aadhar, S. and Mishra, V.: High-resolution near real-time drought monitoring in South Asia,
381 *Sci. data*, 4, 170145, 2017.

382 Abbas, S., Nichol, J. E., Qamer, F. M. and Xu, J.: Characterization of drought development
383 through remote sensing: A case study in Central Yunnan, China. *Remote sensing*, 2014, 6,
384 4998-5018, *Remote Sens.*, 6(6), 4998–5018, doi:10.3390/rs6064998, 2014.

385 Agam, N., Kustas, W. P., Anderson, M. C., Li, F. and Neale, C. M. U.: A vegetation index
386 based technique for spatial sharpening of thermal imagery, *Remote Sens. Environ.*, 107(4),
387 545–558, 2007.

388 Agutu, N. O., Awange, J. L., Zerihun, A., Ndehedehe, C. E., Kuhn, M. and Fukuda, Y.:
389 Assessing multi-satellite remote sensing, reanalysis, and land surface models' products in
390 characterizing agricultural drought in East Africa, *Remote Sens. Environ.*, 194, 287–302,
391 2017.

392 Ambika, A. K. and Mishra, V.: Observational evidence of irrigation influence on vegetation
393 health and land surface temperature in India, *Geophys. Res. Lett.*, 2019.

394 Anderson, M. C., Norman, J. M., Kustas, W. P., Houborg, R., Starks, P. J. and Agam, N.: A
395 thermal-based remote sensing technique for routine mapping of land-surface carbon, water
396 and energy fluxes from field to regional scales, *Remote Sens. Environ.*, 112(12), 4227–4241,
397 2008.

398 Bannari, A., Morin, D., Bonn, F. and Huete, A.: A review of vegetation indices, *Remote*
399 *Sens. Rev.*, 13(1–2), 95–120, 1995.



- 400 Barker, L. J., Hannaford, J., Chiverton, A. and Svensson, C.: From meteorological to
401 hydrological drought using standardized indicators, *Hydrol. Earth Syst. Sci.*, 20(6), 2483–
402 2505, 2016.
- 403 Bento, V. A., Gouveia, C. M., DaCamara, C. C. and Trigo, I. F.: A climatological assessment
404 of drought impact on vegetation health index, *Agric. For. Meteorol.*, 259, 286–295, 2018.
- 405 Bhardwaj, K., Shah, D., Aadhar, S. and Mishra, V.: Propagation of meteorological to
406 hydrological droughts in India, *J. Geophys. Res. Atmos.*, 125(22), e2020JD033455, 2020.
- 407 Dai, A.: Drought under global warming: a review, *Wiley Interdiscip. Rev. Clim. Chang.*,
408 2(1), 45–65, 2011.
- 409 Didan, K., Munoz, A. B., Solano, R. and Huete, A.: MODIS vegetation index user's guide
410 (MOD13 Series), Univ. Arizona Veg. Index Phenol. Lab, 2015.
- 411 Drury, S. A.: Image interpretation in geology, 1987.
- 412 Gao, X., Huete, A. R., Ni, W. and Miura, T.: Optical–biophysical relationships of vegetation
413 spectra without background contamination, *Remote Sens. Environ.*, 74(3), 609–620, 2000.
- 414 García-León, D., Contreras, S. and Hunink, J.: Comparison of meteorological and satellite-
415 based drought indices as yield predictors of Spanish cereals, *Agric. Water Manag.*, 213, 388–
416 396, 2019.
- 417 Godfray, H. C. J., Beddington, J. R., Crute, I. R., Haddad, L., Lawrence, D., Muir, J. F.,
418 Pretty, J., Robinson, S., Thomas, S. M. and Toulmin, C.: Food security: the challenge of
419 feeding 9 billion people, *Science* (80-.), 327(5967), 812–818, 2010.
- 420 Gomes, A. C. C., Bernardo, N. and Alcântara, E.: Accessing the southeastern Brazil 2014
421 drought severity on the vegetation health by satellite image, *Nat. Hazards*, 89(3), 1401–1420,
422 2017.
- 423 Gowda, P. H., Chavez, J. L., Colaizzi, P. D., Evett, S. R., Howell, T. A. and Tolck, J. A.:
424 Remote sensing based energy balance algorithms for mapping ET: Current status and future
425 challenges, *Trans. ASABE*, 50(5), 1639–1644, 2007.
- 426 Gurung, R. B., Breidt, F. J., Dutin, A. and Ogle, S. M.: Predicting Enhanced Vegetation
427 Index (EVI) curves for ecosystem modeling applications, *Remote Sens. Environ.*, 113(10),
428 2186–2193, 2009.
- 429 Gutman, G. G.: On the monitoring of land surface temperatures with the NOAA/AVHRR:
430 removing the effect of satellite orbit drift, *Int. J. Remote Sens.*, 20(17), 3407–3413, 1999.
- 431 Hao, C., Zhang, J. and Yao, F.: Combination of multi-sensor remote sensing data for drought
432 monitoring over Southwest China, *Int. J. Appl. Earth Obs. Geoinf.*, 35, 270–283, 2015.
- 433 Hao, Z. and AghaKouchak, A.: Multivariate standardized drought index: a parametric multi-
434 index model, *Adv. Water Resour.*, 57, 12–18, 2013.
- 435 Huete, A., Didan, K., Miura, T., Rodriguez, E. P., Gao, X. and Ferreira, L. G.: Overview of
436 the radiometric and biophysical performance of the MODIS vegetation indices, *Remote Sens.*
437 *Environ.*, 83(1–2), 195–213, 2002.
- 438 Jeganathan, C., Hamm, N. A. S., Mukherjee, S., Atkinson, P. M., Raju, P. L. N. and
439 Dadhwal, V. K.: Evaluating a thermal image sharpening model over a mixed agricultural
440 landscape in India, *Int. J. Appl. Earth Obs. Geoinf.*, 13(2), 178–191, 2011.



- 441 Jiao, W., Tian, C., Chang, Q., Novick, K. A. and Wang, L.: A new multi-sensor integrated
442 index for drought monitoring, *Agric. For. Meteorol.*, 268, 74–85, 2019.
- 443 Jiao, W., Wang, L. and McCabe, M. F.: Multi-sensor remote sensing for drought
444 characterization: current status, opportunities and a roadmap for the future, *Remote Sens.*
445 *Environ.*, 256, 112313, 2021.
- 446 Kogan, F., Salazar, L. and Roytman, L.: Forecasting crop production using satellite-based
447 vegetation health indices in Kansas, USA, *Int. J. Remote Sens.*, 33(9), 2798–2814, 2012.
- 448 Kogan, F. N.: Application of vegetation index and brightness temperature for drought
449 detection, *Adv. Sp. Res.*, 15(11), 91–100, 1995a.
- 450 Kogan, F. N.: Droughts of the late 1980s in the United States as derived from NOAA polar-
451 orbiting satellite data, *Bull. Am. Meteorol. Soc.*, 76(5), 655–668, 1995b.
- 452 Kustas, W. P., Norman, J. M., Anderson, M. C. and French, A. N.: Estimating subpixel
453 surface temperatures and energy fluxes from the vegetation index–radiometric temperature
454 relationship, *Remote Sens. Environ.*, 85(4), 429–440, 2003.
- 455 Li, H., Sun, D., Yu, Y., Wang, H., Liu, Y., Liu, Q., Du, Y., Wang, H. and Cao, B.: Evaluation
456 of the VIIRS and MODIS LST products in an arid area of Northwest China, *Remote Sens.*
457 *Environ.*, 142, 111–121, 2014.
- 458 Liu, Y., Hiyama, T. and Yamaguchi, Y.: Scaling of land surface temperature using satellite
459 data: A case examination on ASTER and MODIS products over a heterogeneous terrain area,
460 *Remote Sens. Environ.*, 105(2), 115–128, 2006.
- 461 Lloyd-Hughes, B.: The impracticality of a universal drought definition, *Theor. Appl.*
462 *Climatol.*, 117(3), 607–611, 2014.
- 463 Van Loon, A. F.: Hydrological drought explained, *Wiley Interdiscip. Rev. Water*, 2(4), 359–
464 392, 2015.
- 465 Van Loon, A. F. and Laaha, G.: Hydrological drought severity explained by climate and
466 catchment characteristics, *J. Hydrol.*, 526, 3–14, 2015.
- 467 Mahto, S. S. and Mishra, V.: Dominance of summer monsoon flash droughts in India,
468 *Environ. Res. Lett.*, 2020.
- 469 Martens, B., Miralles, D. G., Lievens, H., Van Der Schalie, R., De Jeu, R. A. M., Fernández-
470 Prieto, D., Beck, H. E., Dorigo, W. A. and Verhoest, N. E. C.: GLEAM v3: Satellite-based
471 land evaporation and root-zone soil moisture, *Geosci. Model Dev.*, 10(5), 1903–1925, 2017.
- 472 McKee, T. B., Doesken, N. J. and Kleist, J.: The relationship of drought frequency and
473 duration to time scales, in *Proceedings of the 8th Conference on Applied Climatology*, vol.
474 17, pp. 179–183, California., 1993.
- 475 Mishra, A. K. and Singh, V. P.: A review of drought concepts, *J. Hydrol.*, 391(1–2), 202–
476 216, 2010.
- 477 Mishra, V.: Long-term (1870–2018) drought reconstruction in context of surface water
478 security in India, *J. Hydrol.*, 580, 124228, 2020.
- 479 Mishra, V., Smoliak, B. V., Lettenmaier, D. P. and Wallace, J. M.: A prominent pattern of
480 year-to-year variability in Indian Summer Monsoon Rainfall, *Proc. Natl. Acad. Sci.*, 109(19),
481 7213–7217, doi:10.1073/pnas.1119150109, 2012.



- 482 Mishra, V., Aadhar, S., Asoka, A., Pai, S. and Kumar, R.: On the frequency of the 2015
483 monsoon season drought in the Indo-Gangetic Plain, *Geophys. Res. Lett.*, 43(23), 12,102-
484 12,112, doi:10.1002/2016GL071407, 2016.
- 485 Mishra, V., Shah, R., Azhar, S., Shah, H., Modi, P. and Kumar, R.: Reconstruction of
486 droughts in India using multiple land-surface models (1951-2015), *Hydrol. Earth Syst. Sci.*,
487 22(4), 2269–2284, doi:10.5194/hess-22-2269-2018, 2018.
- 488 Mishra, V., Aadhar, S. and Mahto, S. S.: Anthropogenic warming and intraseasonal summer
489 monsoon variability amplify the risk of future flash droughts in India, *Npj Clim. Atmos. Sci.*,
490 4(1), 1–10, 2021.
- 491 Mooley, D. A. and Parthasarathy, B.: Droughts and floods over India in summer monsoon
492 seasons 1871–1980, in *Variations in the global water budget*, pp. 239–252, Springer., 1983.
- 493 Mu, Q., Zhao, M., Kimball, J. S., McDowell, N. G. and Running, S. W.: A remotely sensed
494 global terrestrial drought severity index, *Bull. Am. Meteorol. Soc.*, 94(1), 83–98,
495 doi:10.1175/BAMS-D-11-00213.1, 2013.
- 496 Nichol, J. and Wong, M. S.: Modeling urban environmental quality in a tropical city, *Landsc.*
497 *Urban Plan.*, 73(1), 49–58, 2005.
- 498 Orhan, O., Ekercin, S. and Dadaser-Celik, F.: Use of landsat land surface temperature and
499 vegetation indices for monitoring drought in the Salt Lake Basin Area, Turkey, *Sci. World J.*,
500 2014, 2014.
- 501 Palmer, W. C.: *Meteorological drought*, US Department of Commerce, Weather Bureau.,
502 1965.
- 503 Pardo-Iguzquiza, E., Rodríguez-Galiano, V. F., Chica-Olmo, M. and Atkinson, P. M.: Image
504 fusion by spatially adaptive filtering using downscaling cokriging, *ISPRS J. Photogramm.*
505 *Remote Sens.*, 66(3), 337–346, 2011.
- 506 Pardo-Igúzquiza, E., Chica-Olmo, M. and Atkinson, P. M.: Downscaling cokriging for image
507 sharpening, *Remote Sens. Environ.*, 102(1–2), 86–98, doi:10.1016/j.rse.2006.02.014, 2006.
- 508 Prasad, A. K., Chai, L., Singh, R. P. and Kafatos, M.: Crop yield estimation model for Iowa
509 using remote sensing and surface parameters, *Int. J. Appl. earth Obs. Geoinf.*, 8(1), 26–33,
510 2006.
- 511 Rahman, A., Roytman, L., Krakauer, N. Y., Nizamuddin, M. and Goldberg, M.: Use of
512 vegetation health data for estimation of Aus rice yield in Bangladesh, *Sensors*, 9(4), 2968–
513 2975, 2009.
- 514 Rodríguez-Galiano, V., Pardo-Iguzquiza, E., Sanchez-Castillo, M., Chica-Olmo, M. and
515 Chica-Rivas, M.: Downscaling Landsat 7 ETM+ thermal imagery using land surface
516 temperature and NDVI images, *Int. J. Appl. Earth Obs. Geoinf.*, 18(1), 515–527,
517 doi:10.1016/j.jag.2011.10.002, 2012.
- 518 Rojas, O., Vrieling, A. and Rembold, F.: Assessing drought probability for agricultural areas
519 in Africa with coarse resolution remote sensing imagery, *Remote Sens. Environ.*, 115(2),
520 343–352, doi:10.1016/j.rse.2010.09.006, 2011.
- 521 Roxy, M. K., Ritika, K., Terray, P., Murtugudde, R., Ashok, K. and Goswami, B. N.: Drying
522 of Indian subcontinent by rapid Indian Ocean warming and a weakening land-sea thermal
523 gradient, *Nat. Commun.*, 6, 7423 [online] Available from:



- 524 <https://doi.org/10.1038/ncomms8423>, 2015.
- 525 Saha, T. R., Shrestha, P. K., Rakovec, O., Thober, S. and Samaniego, L.: A drought
526 monitoring tool for South Asia, *Environ. Res. Lett.*, 16(5), 54014, 2021.
- 527 Sánchez, N., González-Zamora, Á., Piles, M. and Martínez-Fernández, J.: A new Soil
528 Moisture Agricultural Drought Index (SMADI) integrating MODIS and SMOS products: A
529 case of study over the Iberian Peninsula, *Remote Sens.*, 8(4), doi:10.3390/rs8040287, 2016.
- 530 Seneviratne, S. I., Corti, T., Davin, E. L., Hirschi, M., Jaeger, E. B., Lehner, I., Orlowsky, B.
531 and Teuling, A. J.: Investigating soil moisture–climate interactions in a changing climate: A
532 review, *Earth-Science Rev.*, 99(3–4), 125–161, 2010.
- 533 Seyednasrollah, B., Domec, J.-C. and Clark, J. S.: Spatiotemporal sensitivity of thermal stress
534 for monitoring canopy hydrological stress in near real-time, *Agric. For. Meteorol.*, 269, 220–
535 230, 2019.
- 536 Shah, D., Shah, H. L., Dave, H. M. and Mishra, V.: Contrasting influence of human activities
537 on agricultural and hydrological droughts in India, *Sci. Total Environ.*, 774, 144959, 2021.
- 538 Shah, R. D. and Mishra, V.: Development of an experimental near-real-time drought monitor
539 for India, *J. Hydrometeorol.*, 16(1), 327–345, 2015.
- 540 Souza, A. G. S. S., Neto, A. R. and de Souza, L. L.: Soil moisture-based index for
541 agricultural drought assessment: SMADI application in Pernambuco State-Brazil, *Remote
542 Sens. Environ.*, 252, 112124, 2021.
- 543 Stathopoulou, M. and Cartalis, C.: Downscaling AVHRR land surface temperatures for
544 improved surface urban heat island intensity estimation, *Remote Sens. Environ.*, 113(12),
545 2592–2605, 2009.
- 546 Takeuchi, W., Darmawan, S., Shofiyati, R., Khiem, M. V., Oo, K. S., Pimple, U. and Heng,
547 S.: Near-real time meteorological drought monitoring and early warning system for croplands
548 in asia, in *Asian Conference on Remote Sensing 2015: Fostering Resilient Growth in Asia*,
549 vol. 1, pp. 171–178, Citeseer., 2015.
- 550 Tomlinson, C. J., Chapman, L., Thornes, J. E. and Baker, C.: Remote sensing land surface
551 temperature for meteorology and climatology: a review, *Meteorol. Appl.*, 18(3), 296–306,
552 2011.
- 553 Vicente-Serrano, S. M., Beguería, S. and López-Moreno, J. I.: A multiscalar drought index
554 sensitive to global warming: the standardized precipitation evapotranspiration index, *J. Clim.*,
555 23(7), 1696–1718, 2010.
- 556 Vicente-Serrano, S. M., Miralles, D. G., Domínguez-Castro, F., Azorin-Molina, C., El
557 Kenawy, A., Mcvicar, T. R., Tomás-Burguera, M., Beguería, S., Maneta, M. and Peña-
558 Gallardo, M.: Global assessment of the standardized evapotranspiration deficit index (SEDI)
559 for drought analysis and monitoring, *J. Clim.*, 31(14), 5371–5393, doi:10.1175/JCLI-D-17-
560 0775.1, 2018.
- 561 Wan, Z.: MODIS land surface temperature products users' guide, *Inst. Comput. Earth Syst.*
562 *Sci. Univ. Calif. St. Barbar. CA, USA*, 805, 2006.
- 563 Wang, Z. and Bovik, A. C.: A universal image quality index, *IEEE Signal Process. Lett.*,
564 9(3), 81–84, 2002.



565 Wang, Z., Bovik, A. C., Sheikh, H. R. and Simoncelli, E. P.: Image quality assessment: from
 566 error visibility to structural similarity, *IEEE Trans. image Process.*, 13(4), 600–612, 2004.

567 Wilhite, D. A.: Drought and water crises: science, technology, and management issues, Crc
 568 Press., 2005.

569 Wilhite, D. A. and Glantz, M. H.: Understanding: the drought phenomenon: the role of
 570 definitions, *Water Int.*, 10(3), 111–120, 1985.

571 Wilhite, D. A., Hayes, M. J., Knutson, C. and Smith, K. H.: Planning for Drought: Moving
 572 From Crisis to Risk Management 1, *JAWRA J. Am. Water Resour. Assoc.*, 36(4), 697–710,
 573 2000.

574 Yu, M., Li, Q., Hayes, M. J., Svoboda, M. D. and Heim, R. R.: Are droughts becoming more
 575 frequent or severe in China based on the standardized precipitation evapotranspiration index:
 576 1951–2010?, *Int. J. Climatol.*, 34(3), 545–558, 2014.

577 Zhou, S., Park Williams, A., Berg, A. M., Cook, B. I., Zhang, Y., Hagemann, S., Lorenz, R.,
 578 Seneviratne, S. I. and Gentine, P.: Land–atmosphere feedbacks exacerbate concurrent soil
 579 drought and atmospheric aridity, *Proc. Natl. Acad. Sci. U. S. A.*, 116(38), 18848–18853,
 580 doi:10.1073/pnas.1904955116, 2019.

581 Table 1: List of acronyms used in the study

Variable Name	Acronyms
Land Surface Temperature	LST
Enhanced Vegetation Index	EVI
Soil Moisture Agriculture Drought Index	SMADI
Normalized Vegetation Supply Water Index	NVSWI
Vegetation Health Index	VHI
Vegetation Condition Index	VCI
Temperature Condition Index	TCI
Moderate Resolution Imaging Spectroradiometer	MODIS
Normalized Difference Vegetation Index	NDVI
Surface Spectral Reflectance of MODIS Red and Near infrared Bands	MOD09Q1
Surface Spectral Reflectance of MODIS Blue Band	MOD09A1
National Oceanic and Atmospheric Administration	NOAA
(NOAA) Star Center for Satellite Application and Research	NSTAR
Advanced Spaceborne Thermal Emission and Reflection Radiometer	ASTER
MODIS Land Surface Temperature and Emissivity	MOD11A2
Shuttle Radar Topography Mission	SRTM
Structural Similarity Index	SSIM
Image Quality Index	IQI
Advanced Very High-Resolution Radiometer	AVHRR
Global Land Evaporation Amsterdam Model	GLEAM
Standardized Evaporation Deficit Index	SEDI
Drought Severity Index	DSI

582
 583
 584
 585
 586



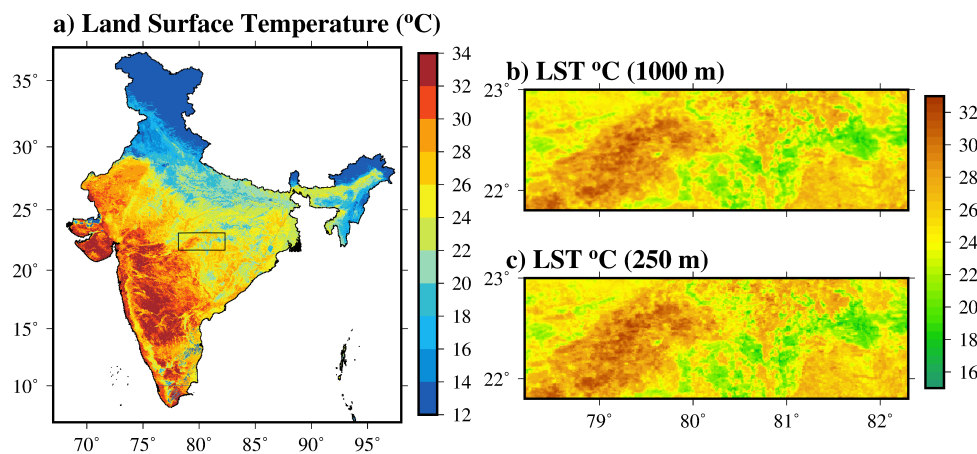
587 Table 2: Summary of dataset used along with their sources

Sl.no	Data set	Derived Variables	Resolution and Duration	Satellite/Data Provider	DOI	Data Link
1	MOD09 Q1	Surface reflectance red and near infrared bands	250 m & 2000-2017	Moderate Resolution Imaging Spectroradiometer	https://doi.org/10.5067/MODIS/MOD09Q1.006	https://e4ftl01.cr.usgs.gov/MOLT/MOD09Q1.006/
2	MOD09 A1	Surface reflectance blue band	250 m & 2000-2017	Moderate Resolution Imaging Spectroradiometer	https://doi.org/10.5067/MODIS/MOD09A1.006	https://e4ftl01.cr.usgs.gov/MOLT/MOD09A1.006/
3	MOD11 A2	Land Surface Temperature	1000 m & 2000-2017	Moderate Resolution Imaging Spectroradiometer	https://doi.org/10.5067/MODIS/MOD11A2.006	https://e4ftl01.cr.usgs.gov/MOLT/MOD11A2.006/
4	SRTM	Digital elevation model	90 m & 2000	Shuttle Radar Topography Mission	https://doi.org/10.5066/F7K072R7	https://earthexplorer.usgs.gov/
5	GLEAM	Soil Moisture	0.25° & 2000-2017	The Global Land Evaporation Amsterdam Model	https://doi.org/10.5194/gmd-10-1903-2017	https://www.gleam.eu/
6	SEDI	Drought Index	0.25° & 2000-2016	DIGITAL.CSIC, the institutional repository of the Spanish National Research Council	https://digital.csic.es/handle/10261/160091	https://digital.csic.es/handle/10261/160091
7	DSI	Drought Index	0.05° & 2000-2011	Numerical Terradynamic Simulation Group (NTSG) University of Montana	https://doi.org/10.1175/BAMS-D-11-00213.1	http://files.ntsg.umt.edu/data/NTSG_Products/DSI/

588

589

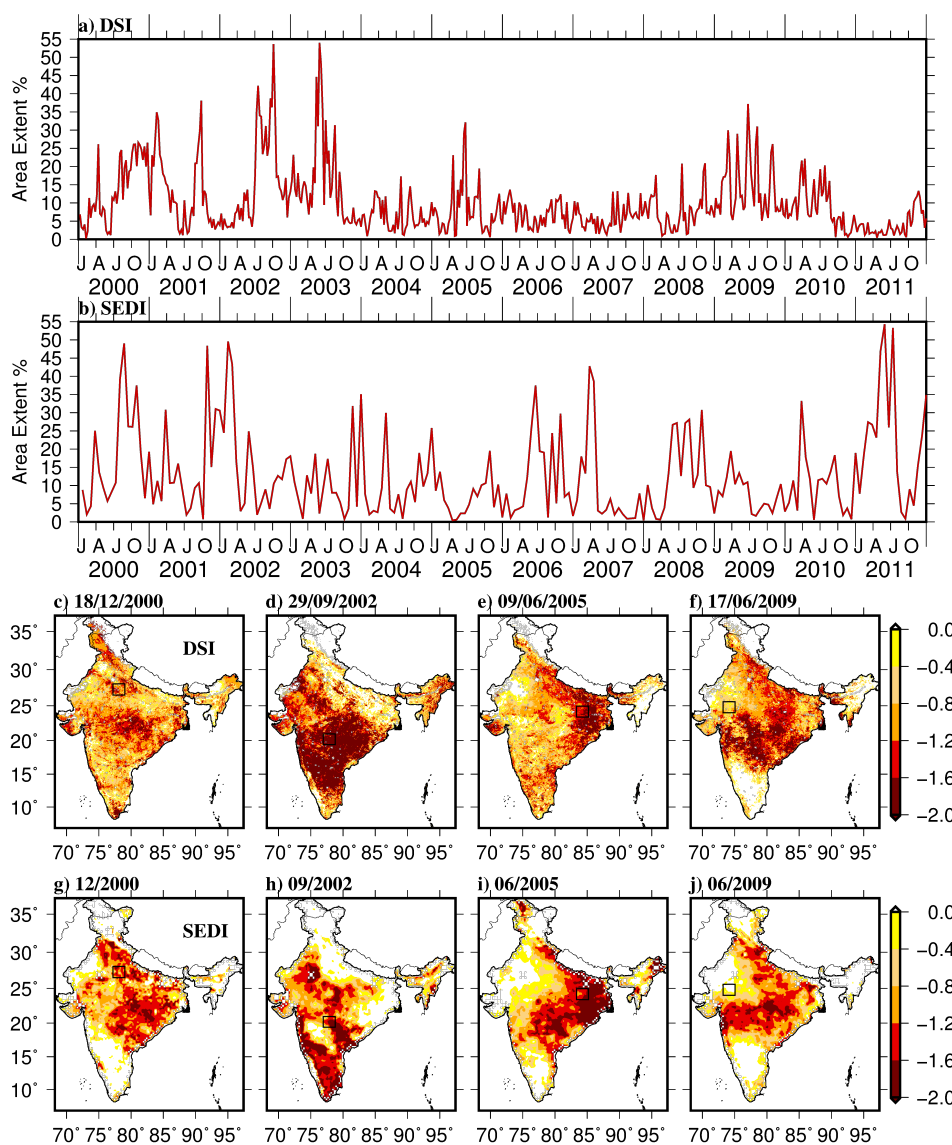
590



591

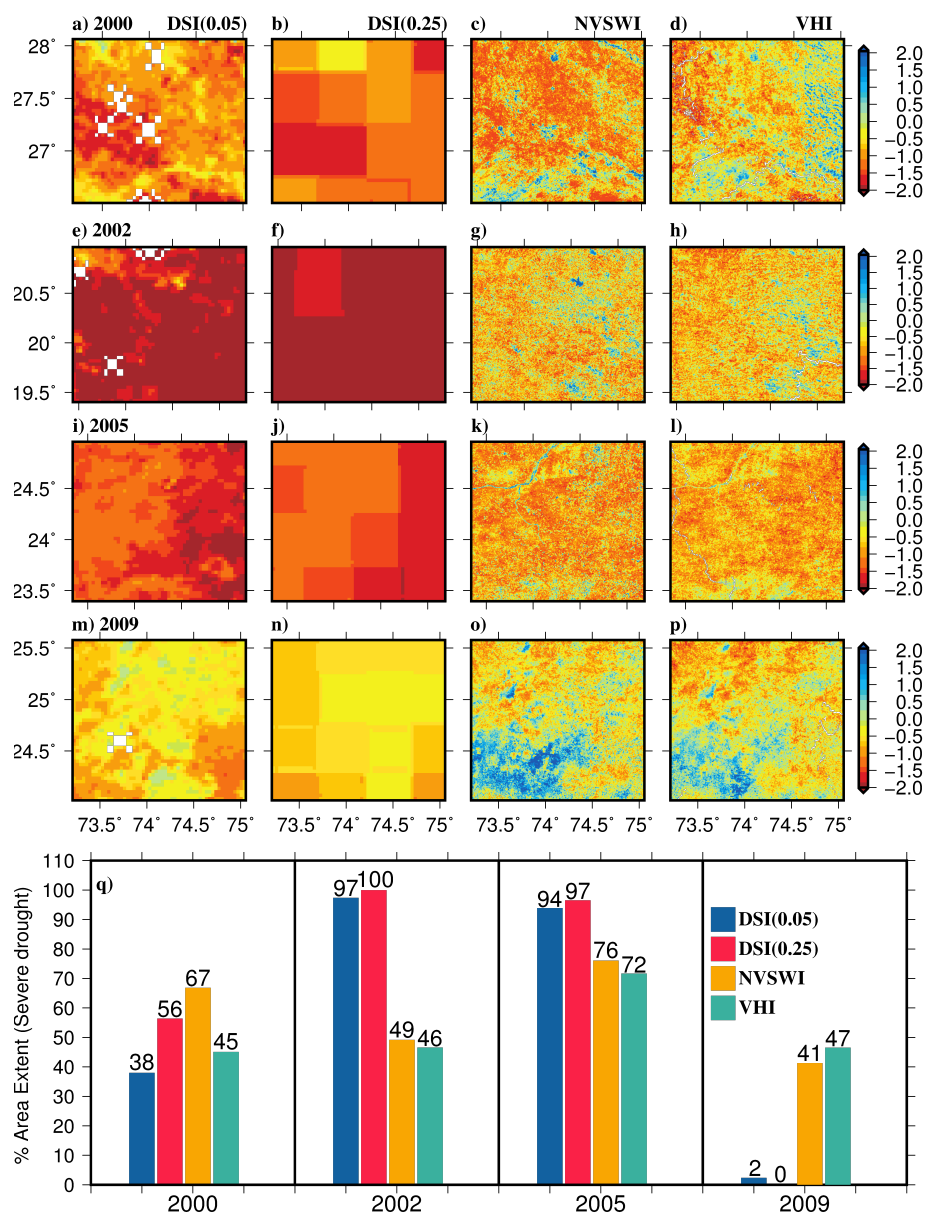


592 Figure 1. (a) Downscaled Land Surface Temperature (LST) at 250 m for February 2000 over
 593 the Indian region, and (b,c) highlights the LST at 1000 m from the MOD11A2 and
 594 downscaled LST at 250 m for central India. The black box in (a) is considered to compare the
 595 spatial coherence and luminance of the low (1000 m) and high (250 m) resolution datasets.



596

597 Figure 2. (a, b) Percentage area in severe drought condition over the Indian region for the
 598 2000-2011 period, (c-f) Drought Severity Index (DSI) at 0.05° along the Indian region for the
 599 same period as (a), and (g-j) same as (c-f) but for Standardized Evaporation Deficit Index
 600 (SEDI) at 0.25°. The highlighted black box is chosen based on LULC and agro-ecological
 601 region for the different severe drought events.



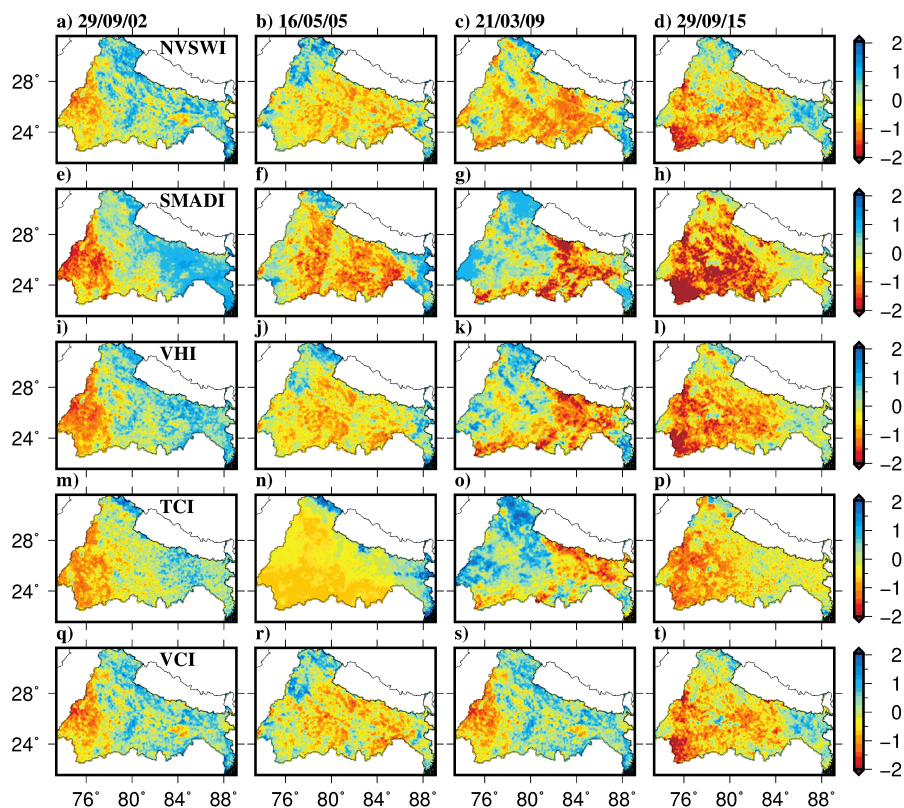
602

603 Figure 3. (a-d), (e-h), (i-l) and (m-p) show drought condition estimated using DSI (0.05), DSI
 604 (0.25), NVSWI (250 m) & VHI (250 m) and (q) is calculated area extent of drought severity
 605 for different periods (2000, 2002, 2005, and 2009). Each column represents different severity
 606 data sets in the order DSI, SEDI, NVSWI and VHI and each row indicates drought period for different
 607 years. Here, drought location is identified from the Figure 2 (c-j) highlighted black box.
 608

609

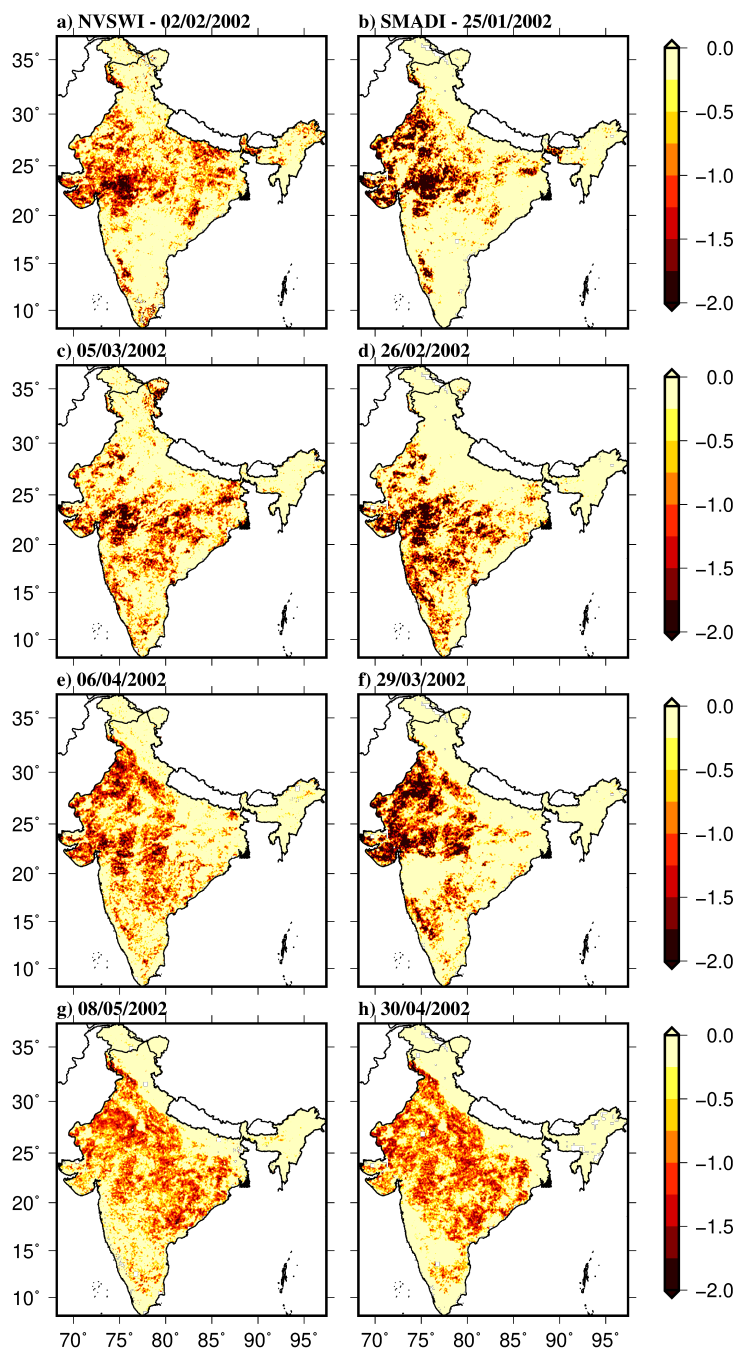


610



611

612 Figure 4. (a-d), (e-h), (i-l), (m-p), and (q-t) show drought conditions estimated using NVSWI
613 (250 m), SMADI (250 m), VHI (250 m), TCI (250 m), and VCI (250 m) and calculated area
614 extent of drought severity for the different period (2002, 2005, 2009 and 2015). Each row
615 represents different data sets in the order NVSWI, SMADI, VHI, TCI, and VCI. Here, the
616 drought severity classifications are identified as incipient drought (between -0.5 and -0.59),
617 mild drought (between -0.6 and -0.89), moderate drought (between -0.9 and -1.19), severe
618 drought (between -1.2 and -1.49), and extreme drought (between -1.5 and less).



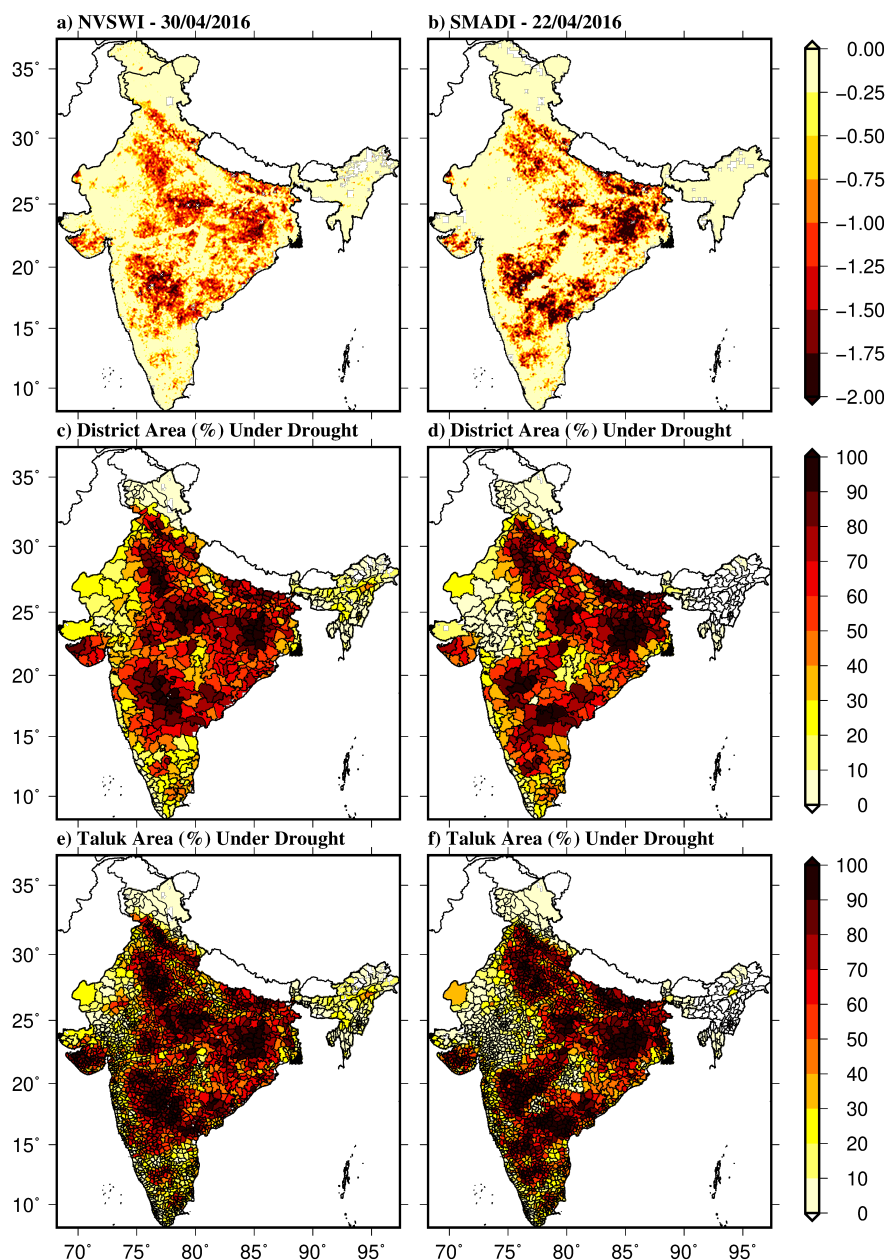
619

620

621 Figure 5: (a-h) Temporal change of drought severity between NVSWI and SMADI at 250 m
622 along the Indian region for the 2002 summer period. Here, the drought severity classifications



623 are identified as incipient drought (between -0.5 and -0.59), mild drought (between -0.6 and -
624 0.89), moderate drought (between -0.9 and -1.19), severe drought (between -1.2 and -1.49),
625 and extreme drought (between -1.5 and less).



626

627

628 Figure 6: District and Taluka level drought monitoring using the NVSWI and SMADI over
629 the Indian Region. (a,b) NVSWI and SMADI calculated for April 2016, (c,d) district (%) area



630 and (e,f) same as (c,d) but for taluka. Here drought values range between moderate and
631 Severe.

632

633

634